Lab on a Chip

Miniaturisation for chemistry, physics, biology, materials science and bioengineering

www.rsc.org/loc

Volume 13 | Number 3 | 7 February 2013 | Pages 313–476

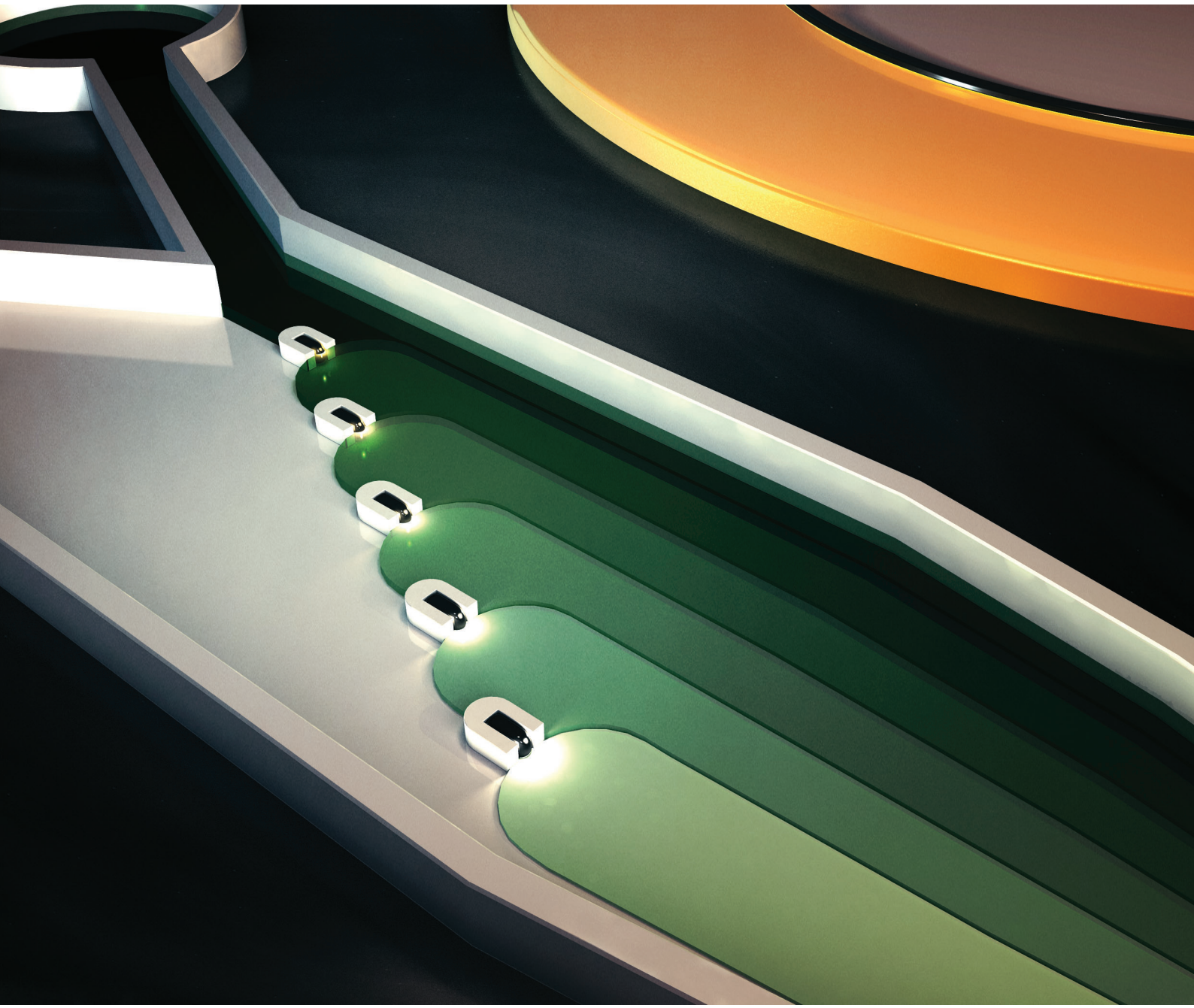

ISSN 1473-0197

RSC Publishing

1473-0197(2013)13:3;1-2

Lab on a Chip

RSC Publishing

COMMUNICATION

Tunable, pulsatile chemical gradient generation *via* acoustically driven oscillating bubbles†

Cite this: *Lab Chip*, 2013, **13**, 328

Received 14th August 2012,
Accepted 5th December 2012

DOI: 10.1039/c2lc40923b

www.rsc.org/loc

Daniel Ahmed,[a] Chung Yu Chan,[a] Sz-Chin Steven Lin,[a] Hari S. Muddana,[b] Nitesh Nama,[a] Stephen J. Benkovic[c] and Tony Jun Huang*[ab]

We present a novel concept of generating both static and pulsatile chemical gradients using acoustically activated bubbles designed in a ladder-like arrangement. Furthermore, by regulating the amplitude of the bubble oscillation, we demonstrate that the chemical gradient profiles can be effectively tuned.

Generating pulsatile chemical gradients in microfluidic devices has important implications for the characterization of dynamic biological[1–4] and chemical processes.[5] Several recent studies have shown that both spatial and temporal characteristics of chemical stimuli play an important role in cell signalling.[6–9] In addition, pulsatile chemical gradients can be useful for high-throughput characterization of cellular processes such as directed migration,[10] differentiation,[11,12] and apoptosis.[13] Existing techniques to generate chemical gradients include the Boyden chamber and its derivatives,[14–16] the micropipette method,[17] and microfluidic-based systems.[18–22] Although all of these methods are capable of generating linear and radial chemical gradient profiles in a static manner, limited research[23–27] has been conducted on dynamic temporal control of chemical gradients.

In this article, we demonstrate that multiple bubbles that are arranged in a ladder-like formation and oscillating in an acoustic field provide a novel and versatile method to generate tunable, pulsatile chemical gradients in microdevices. The bubbles were trapped and supported in the polydimethylsiloxane (PDMS) microfluidic channel using horseshoe structures, a technique previously developed by our group.[28] Each oscillating bubble (Fig. 1a), when activated, mixes the stimulus and buffer solutions locally,[28–33] effectively diluting the stimulant concentration. Subsequent transport of this mixed stimulant to the next bubble in the ladder results in further dilution of the stimulant, thereby generating a spatial gradient of the stimulant across the microchannel. In addition, each of the oscillating bubbles can be activated or deactivated almost instantaneously, facilitating the generation of pulsatile chemical gradients. Furthermore, by controlling the mixing ratio of the stimulant and the buffer, we demonstrate that the chemical gradient profiles can be tuned on-the-fly.

Our experimental setup (Fig. 1a) contains multiple bubbles trapped by horseshoe structures (60 × 90 × 60 μm; see also Supplementary Information). Briefly, a single-layer PDMS channel containing multiple horseshoe structures is bonded to a glass slide, while a piezoelectric transducer is attached adjacent to the channel. After the bubbles were trapped in the horseshoe structures (refer to Video 1 of the Supporting Information† for more details), stimulant (green, Fig. 1a) at the maximum concentration of C_0 was introduced into the channel through

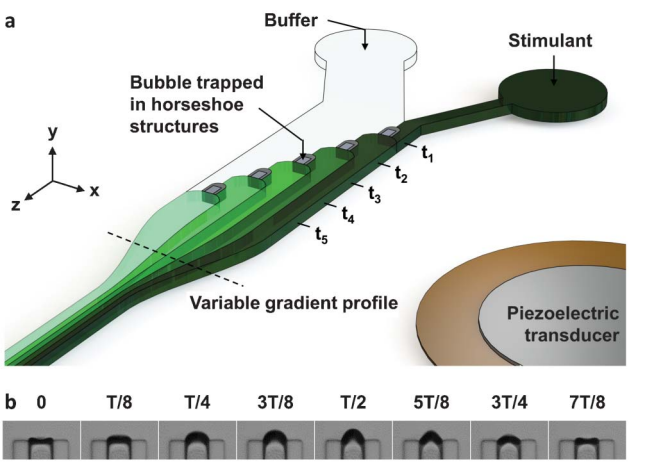

Fig. 1 (a) Schematic of the experimental setup. A piezoelectrical transducer is placed adjacent to the microfluidic device. A chemical gradient profile is established between the co-flowing stimulant and buffer in the microfluidic channel. (b) Image sequence acquired at 200,000 fps to capture one complete cycle of an oscillating bubble trapped within a horseshoe structure.

[a]*Department of Engineering Science and Mechanics, The Pennsylvania State University, University Park, PA 16802, USA. E-mail: junhuang@psu.edu; Fax: +814-865-9974; Tel: +814-863-4209*
[b]*Department of Bioengineering, The Pennsylvania State University, University Park, Pennsylvania, 16802 USA*
[c]*Department of Chemistry, The Pennsylvania State University, University Park, Pennsylvania, 16802 USA*

† Electronic supplementary information (ESI) available: Trapping multiple bubbles within horseshoe structures, videos for pulsatile gradient generation, device fabrication and design, and experimental setup. See DOI: 10.1039/c2lc40923b

the right inlet, while the buffer was infused through the left inlet. Parallel laminar flows of stimulant and buffer across the channel were established. When the bubbles were acoustically activated *via* the piezoelectric transducer at an excitation frequency of 30 kHz, the oscillations of the bubbles exhibited the "microstreaming" phenomenon.[34–40] All the horseshoe structures were designed to be of identical geometry, and as a result the trapped bubbles oscillated at a single resonance frequency. In principle, the acoustic microstreaming is generated due to the nonlinear effects of the oscillatory fluid motion produced by the acoustic waves.[41] The pressure and velocity fluctuations in the liquid near the bubble cause rapid and homogeneous sideward mixing of the co-flowing liquids. As shown in Fig. 1a, at t_1, the stimulant and buffer are mixed by the oscillating bubble nearest the inlets, resulting in a lower concentration, C_1, as the stimulant approaches the second bubble. At t_2, the liquid (after passing the first horseshoe structure) with concentration C_1 is mixed with the buffer in the laminar region resulting in further lower concentration, C_2. As this step-wise dilution of the stimulant progresses, all the liquid is mixed and merged across the channel resulting in a spatial chemical gradient.

Oscillation of bubbles can be tuned directly by controlling the voltage fed into the transducer. As indicated in the experimental results shown in Fig. 2a, the oscillation amplitude responds linearly to the applied voltage in our experiments. As a consequence, the mixing distance, *d*, varies linearly with increasing applied voltage (Fig. 2a). Since bubbles trapped within the horseshoe structures are organized in a ladder-like formation with each one offsetting from the last one by a length, *l*, different applied voltage allows different mixing distance, enabling us to achieve different chemical profiles. For a ladder-like horseshoe structure formation used in this article (detailed design is provided in Fig. S1–S3 of the ESI†), we simulated the generated gradient profiles at different mixing distances using a home-made MATLAB code. The code considers both diffusion and bubble-enabled mixing effects. It also makes assumptions of homogeneous mixing, uniform flow velocity along X-coordinates, and the absence of crosstalk between bubbles. The simulated results for mixing distances of 250 μm and 375 μm are shown in Fig. 2c and 2d, respectively. The simulated chemical gradient profiles measured at downstream (noted by the dashed line in Fig. 2c) at mixing distance ranging from 250 μm to 600 μm are summarised in Fig. 2b. Clearly we can observe the relationship between the shape of generated gradient profile and the mixing distance that is controlled by the applied voltage. Therefore by adjusting the voltage applied we can dynamically control the spatial and temporal chemical gradient profile.

To experimentally prove the effectiveness of our method, we used Dextran-FITC (stimulant) and phosphate buffered saline (buffer) solutions to generate different spatial and temporal concentration profiles across the microfluidic channel. Owing to the low Reynolds number[42–47] in the microfluidic channel, laminar flow of the inflowing stimulant and buffer solutions was established during the "off" state of the transducer, as shown in Fig. 3a. Once the transducer was turned "on", all bubbles trapped within the horseshoe structures were excited simultaneously. The streaming and sideward mixing of the liquids at the trapped bubbles in a stepwise fashion resulted in a gradient of the stimulant. Fig. 3b shows the gradient generated around the horseshoe structures and the region far away from the bubbles. We adjusted the voltage such that a mixing ratio of 1 : 1 was achieved between subsequent bubbles, ensuring an exponential decay chemical profile. Fluorescence distribution across the channel at positions 1–6 (after passing each bubble, indicated in Fig. 3b) is shown in Fig. 3e. We observed a step-like intensity function at position 1 due to absence of mixing between the Dextran-FITC and PBS solution. At position 2, Dextran-FITC and PBS solutions were mixed in the region between the front end of the first horseshoe structure and the rear end of the second horseshoe structure. Similarly, the subsequent oscillating bubble progressively mixed and diluted the Dextran-FITC until an exponential decay gradient profile was established at position 6, as depicted in Fig. 3e (yellow line). As the stimulant approaches the rear end of the channel, diffusion-induced mixing of the stimulant and buffer solutions results in smoothening of the generated chemical gradient, as shown in Fig. 3f (V_{PP} = 12 V). The channel width is decreased from 1.6 mm to 0.6 mm for future cell studies under higher objectives. The measured intensity profiles fit well to a first-order exponential decay function, confirming that a 1 : 1 mixing ratio of the subsequent bubbles ensures an exponential gradient profile.

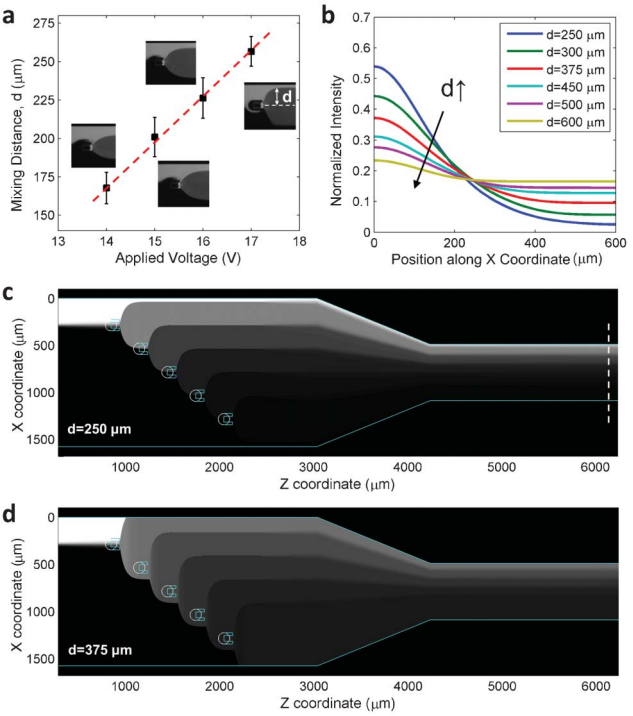

Fig. 2 (a) Experimental results of mixing distance (*d*) as a function of applied voltage (*d* is experimentally measured from the center of the horseshoe structure to the region where no mixing occurs). (b) Simulation results show the dynamic gradient profiles generated when the mixing distance is varied. (c) and (d) Simulation results show the generation of chemical gradients with different mixing distance (*d* = 250 μm and 375 μm, respectively) within the channel.

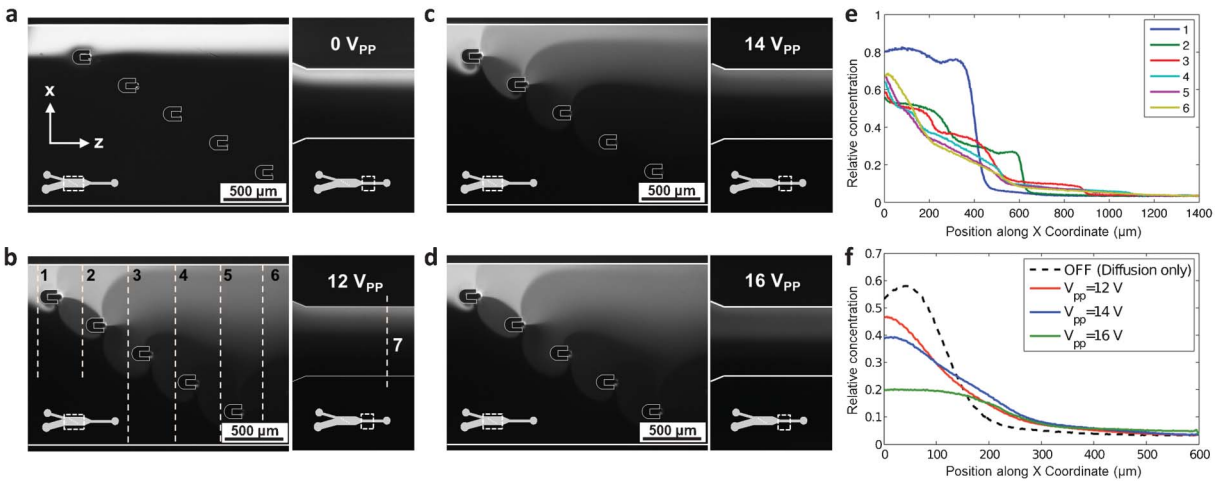

Fig. 3 Characterization of concentration gradient profiles within the microfluidic channel. (a) Images show the interface of the FITC-dextran and PBS at the first horseshoe structure, and the rear region when the piezoelectric transducer is turned off. (b) Six different positions (1–6) were analyzed across and along the channel, during the on-state of the piezoelectric transducer at 12 V_{PP}. Each dotted-line was chosen at the rear end of the horseshoe structures. (c) and (d) Different concentration gradient profiles generated when the applied voltage changed from 14 V_{PP} to 16 V_{PP}. (e) Relative concentration with respect to input concentration (1 mg ml^{-1}) profiles for the corresponding positions in (b) were measured by Image J and plotted to reveal the formation of concentration gradient profile. The change in concentration profile from position 1 to 6 was due to subsequent mixing and merging of co-flowing liquids passed around each of the bubbles. (f) A graph showing different concentration gradient profiles at the rear end of the channel (position 7) in (b), (c), and (d) respectively.

We further demonstrate that different gradient profiles can be obtained by altering the mixing distance *via* changing the applied voltage from the function generator. Fig. 3c and 3d showed that different gradient profiles were generated at 14 V_{pp} and 16 V_{pp}, respectively; the corresponding intensity profiles were shown in Fig. 3f. When the applied voltage varied from 12 V_{pp} to 14 V_{pp}, the mixing distance changed accordingly giving rise to a steeper gradient profile. Similarly, as the applied voltage is increased to 16 V_{pp}, the stronger acoustic streaming results in even higher mixing distance (Fig. 3d). Therefore, the obtained gradient profile is gradual and tended to be sigmoidal like. These results show that our approach has excellent flexibility in tuning chemical profiles.

Besides the capability to produce different gradient profiles, our device is also capable of generating pulsatile gradients at frequencies as high as 0.1 Hz (Note: the excitation frequency of the bubble is at 30 kHz). Fig. 4 shows the fluorescent intensity profiles at positions 1–5 (see inset) at different time values when a pulsing signal from the function generator was used to trigger the formation of the gradient. Evidently pulsing gradient profiles can be generated far away from the acoustic streaming region, thereby removing any shear stress developed by the oscillating bubble.

In conclusion, we have successfully demonstrated the generation of spatial and temporal chemical gradient profiles using acoustically driven oscillating bubbles positioned in a ladder-like formation. Simply changing the applied voltage can dynamically tune the generated chemical gradient profiles, both spatially and temporally. Furthermore, it is possible to obtain more complex and abundant chemical profiles through changing the design of the ladder-like formation. We believe that our acoustofluidic-based method of generating chemical gradient will be invaluable in many chemical and biological studies and applications, such as investigating cell chemotaxis, differentiation, and migration in dynamic chemical environment.

Acknowledgements

This research was supported by National Institutes of Health (NIH) Director's New Innovator Award (1DP2OD007209-01), National Science Foundation (NSF), and the Penn State Center for Nanoscale Science (MRSEC). Components of this work were conducted at the Penn State node of the NSF-funded National Nanotechnology Infrastructure Network. We thank Joey Rufo and Igor I-Kao Chiang for their helpful discussion.

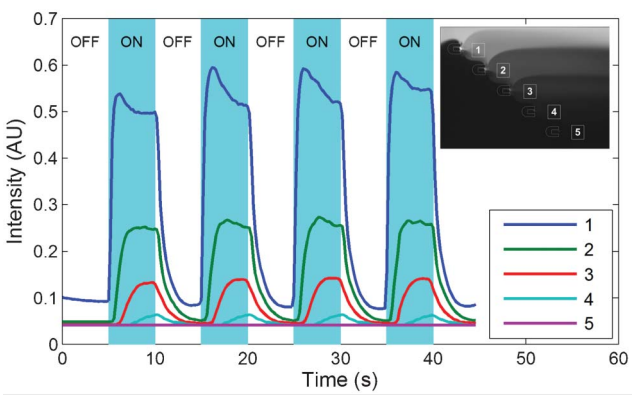

Fig. 4 Experimental results show the pulsing of the gradient at different positions across the channel at a frequency of 0.1 Hz. Fluorescent intensities were measured and analyzed at positions 1–5 (see inset) during the on and off state of the transducer.

References

1 T. S. Shimizu, Y. Tu and H. C. Berg, *Mol. Syst. Biol.*, 2010, **6**, 382.
2 O. Lipan and W. H. Wong, *Proc. Natl. Acad. Sci. U. S. A.*, 2005, **102**, 7063–8.
3 D. Irimia, *Annu. Rev. Biomed. Eng.*, 2010, **12**, 259–286.
4 B. Meier, A. Zielinski, C. Weber, D. Arcizet, S. Youssef, T. Franosch, J. O. Rädler and D. Heinrich, *Proc. Natl. Acad. Sci. U. S. A.*, 2011, **108**, 11417–22.
5 H. Song and R. F. Ismagilov, *J. Am. Chem. Soc.*, 2003, **125**, 14613–9.
6 N. Yosef and A. Regev, *Cell*, 2011, **144**, 886–896.
7 B. N. Kholodenko, J. F. Hancock and W. Kolch, *Nat. Rev. Mol. Cell Biol.*, 2010, **11**, 414–426.
8 J. Li, E. Rose, D. Frances, Y. Sun and L. You, *J. Biomech.*, 2012, **45**, 247–251.
9 J. Kim, I. Hwang, D. Britain, T. D. Chung, Y. Sun and D.-H. Kim, *Lab Chip*, 2011, **11**, 3941.
10 N. Li Jeon, H. Baskaran, S. K. W. Dertinger, G. M. Whitesides, L. Van de Water and M. Toner, *Nature Biotechnology*, 2002, **20**, 826–30.
11 J. O. Gordeladze, F. Djouad, J.-M. Brondello, D. Noël, I. Duroux-Richard, F. Apparailly and C. Jorgensen, *Acta Pharmacol. Sin.*, 2009, **30**, 1369–84.
12 A. Tourovskaia, X. Figueroa-Masot and A. Folch, *Lab Chip*, 2005, **5**, 14–9.
13 D. Wlodkowic, J. Skommer, S. Faley, Z. Darzynkiewicz and J. M. Cooper, *Exp. Cell Res.*, 2009, **315**, 1706–14.
14 S. Boyden, *J. Exp. Med.*, 1961, **115**, 453–466.
15 S. H. Zigmond, *J. Cell Biol.*, 1977, **75**, 606–616.
16 T. M. Keenan and A. Folch, *Lab Chip*, 2008, **8**, 34–57.
17 A. Ainla, E. T. Jansson, N. Stepanyants, O. Orwar and A. Jesorka, *Anal. Chem.*, 2010, **82**, 4529–36.
18 N. L. Jeon, S. K. W. Dertinger, D. T. Chiu, I. S. Choi, A. D. Stroock and G. M. Whitesides, *Langmuir*, 2000, **16**, 8311–8316.
19 D. Irimia, D. A. Geba and M. Toner, *Anal. Chem.*, 2006, **78**, 3472–3477.
20 D. M. Cate, C. G. Sip and A. Folch, *Biomicrofluidics*, 2010, **4**(4), 44105.
21 Š. Selimović, W. Y. Sim, S. B. Kim, Y. H. Jang, W. G. Lee, M. Khabiry, H. Bae, S. Jambovane, J. W. Hong and A. Khademhosseini, *Anal. Chem.*, 2011, **83**(6), 2020–2028.
22 A. Seidi, H. Kaji, N. Annabi, S. Ostrovidov, M. Ramalingam and A. Khademhosseini, *Biomicrofluidics*, 2011, **5**, 022214.
23 H. Kress, J.-G. Park, C. O. Mejean, J. D. Forster, J. Park, S. S. Walse, Y. Zhang, D. Wu, O. D. Weiner, T. M. Fahmy and E. R. Dufresne, *Nat. Methods*, 2009, **6**, 905–9.
24 C. Beta, D. Wyatt, W.-jan Rappel and E. Bodenschatz, *Anal. Chem.*, 2007, **79**, 3940–3944.
25 B. Sun and D. T. Chiu, *Langmuir*, 2004, **20**, 4614–4620.
26 D. Irimia, S.-Y. Liu, W. G. Tharp, A. Samadani, M. Toner and M. C. Poznansky, *Lab Chip*, 2006, **6**, 191–8.
27 B. Kuczenski, W. C. Ruder, W. C. Messner and P. R. Leduc, *PLoS One*, 2009, **4**, e4847.
28 D. Ahmed, X. Mao, J. Shi, B. K. Juluri and T. J. Huang, *Lab Chip*, 2009, **9**, 2738–2741.
29 D. Ahmed, X. Mao, B. K. Juluri and T. J. Huang, *Microfluid. Nanofluid.*, 2009, **7**, 727–731.
30 S.S. Wang, Z. J. Jiao, X. Y. Huang, C. Yang and N. T. Nguyen, *Microfluid. Nanofluid.*, 2008, **6**(6), 847–852.
31 S. Wang, X. Huang and C. Yang, *Lab Chip*, 2011, **11**, 2081–2087.
32 A. R. Tovar and A. P. Lee, *Lab Chip*, 2009, **9**, 41–43.
33 A. R. Tovar, M. V. Patel and A. P. Lee, *Microfluid. Nanofluid.*, 2011, **10**, 1269–1278.
34 T. G. Leighton, *The Acoustic Bubble*, Academic Press, London, 1994.
35 P. Tho, R. Manasseh and A. Ooi, *J. Fluid Mech.*, 2007, **576**, 191–233.
36 M. Wiklund, R. Green and M. Ohlin, *Lab Chip*, 2012, **12**, 2438–2451.
37 S. S. Sadhal, *Lab Chip*, 2012, **12**, 2771–2781.
38 A. Hashmi, G. Yu, M. R-Collete, G. Heiman and J. Xu, *Lab Chip*, 2012, **12**, 4216.
39 S.-C. S. Lin, X. Mao and T. J. Huang, *Lab Chip*, 2012, **12**, 2766–2770.
40 J. Shi, S. Yazdi, S.-C. S. Lin, X. Ding, I.-K. Chiang, K. Sharp and T. J. Huang, *Lab Chip*, 2011, **11**, 2319–24.
41 M. S. Longuet-Higgins, *Proc. R. Soc. London, Ser. A*, 1998, **454**, 725–742.
42 X. Mao, B. K. Juluri, M. I. Lapsley, Z. S. Stratton and T. J. Huang, *Microfluid. Nanofluid.*, 2010, **8**, 139–144.
43 P. S. Dittrich and A. Manz, *Nature Rev. Drug Discov.*, 2006, **5**, 2010–2018.
44 X. Ding, S. S. Lin, B. Kiraly, H. Yue, S. Li, I.-K. Chiang, J. Shi, S. J. Benkovic and T. J. Huang, *Proc. Natl. Acad. Sci. U. S. A.*, 2012, **109**, 11105–11109.
45 P. Neuzil, S. Giselbrecht, K. Länge, T. J. Huang and A. Manz, *Nat. Rev. Drug Discovery*, 2012, **11**, 620–632.
46 S. Yang, F. Guo, B. Kiraly, X. Mao, M. Lu and T. J. Huang, *Lab Chip*, 2012, **12**, 2097–2102.
47 X. Mao and T. J. Huang, *Lab Chip*, 2012, **12**, 1412–1416.